# Models for Propagating Facilitation in the Insect Visual System

Pradeep Singh

Computational Science Research Center

San Diego State University

San Diego, California

Spring 2020

# Approval Page

Title: Models for Propagating Facilitation in the Insect Visual System

Author: Pradeep Singh

Date Submitted:

| | |
|---|---|
| Dr. Jose Castillo | |
| Committee Chair | Signature |
| Dr. Patrick Shoemaker | |
| Advisor & Committee Member | Signature |
| Dr. Joseph M. Mahaffy | |
| Committee Member | Signature |

# ACKNOWLEDGEMENTS

First and foremost, I wish to express my sincere gratitude and appreciation to my supervisor, Professor Patrick Shoemaker for the continuous support and guidance in my MS study and research. He convincingly guided and encouraged me to be professional and do the right thing even when the road got tough. Without his persistent help, the goal of this project would not have been realized. I could not have imagined having a better advisor and mentor for my MS study.

Besides my advisor, I would like to thank Professor Jose E. Castillo and all other staff members at Computational Science Research Center, SDSU for providing lab space and other infrastructure support for the duration of this project. I also express my thanks to my lab mates; Johnny Corbino and Angel Boada for helping me in my initial days, proofreading my thesis and giving insightful comments.

I wish to acknowledge the support and great love of my family (and friends), my mother, Malkeet Kaur; my Father, Baljinder Singh and three of my close friends, Sushil Raut, Neha Patil and Akash Revankar. They kept me going on and this work would not have been possible without their support.

Finally, I would like to thanks sponsors of this project as well. This MS Research was supported by the Air Force Office of Scientific Research, USAF, under grant number FA9550-16-1-0153.

# TABLE OF CONTENTS:

# 1. ABSTRACT

Detecting and tracking moving targets within a visual scene is a complex task. Over thousands of years, many species of animals like flying insects have evolved neural mechanisms for tracking path or location of flying targets that move against the visually cluttered background. Small target motion-detecting (STMD) neurons found in the visual pathway of flying insects display remarkable *selectivity* and *sensitivity* to small moving targets and are thought to support these mechanisms. Contributing to their sensitivity is a form of *facilitation*, in which the responsiveness of an STMD is enhanced by prior exposure to a small target moving along a continuous path in visual space. The locus of facilitation in the receptive field is found to be local to the area of the target and to continue propagating in the direction of target motion even after a stimulus ceases.

In this thesis, we are modeling this phenomenon with the propagation of traveling waves in densely interconnected, retinotopic layers of cells. We hypothesize that waves are initiated and reinforced by the presence of a moving target stimulus, and the network, in turn, interacts with STMDs to modulate their excitability. Membrane potentials travel too fast to play this role, so we have studied and modeled propagating *calcium waves* as a possible mechanism. Accordingly, we have proposed two models that could be the biological substrate for this mechanism: 1) a network of astrocyte-like glia cells, and 2) a network of neurons; both in which calcium waves are initiated by target stimuli and propagate via diffusion with the participation of regenerative mechanisms. And finally we show qualitatively and quantitatively how facilitation would look in any such network and discuss range of parameters that would support facilitation mechanism.

## 2. LIST OF TABLES

## 3. LIST OF FIGURES:

# 4. INTRODUCTION

Detecting and tracking moving targets within a visual scene is a complex task, yet it is of great importance to animals that rely on catching/ chasing their targets for food and mating. Over thousands of years many species of animal have evolved neural mechanisms for target analysis. Flying insect species like dragonflies show amazing ability to track the path or location of flying targets that move against the visually cluttered background again and again. It has also been stated that dragonflies capture prey with success rate of 97% even in the presences of some distraction [1].

Small target motion detector neurons (also known as STMDs) are likely to be involved in this behavior as they display an impressive selectivity for small moving objects [2]. As of now two relatively higher-order functions had been identified that appear to support this behavior: One is *selective attention* that allows STMDs to respond to single target at a time [3]; and second is a type of *facilitation* that enhances the response of an STMD to a continuously-moving target [6]. Our project focuses on second mechanism. A number of experiments have been conducted to characterize the process of facilitation and it has been observed that facilitation is predictive in nature [12].

In this project we investigate the predictive aspect of response facilitation by assuming that it might be supported by the propagation of *calcium waves* in a network of astrocyte-like cells or neurons. We model networks of such cells, and then further analysis is done on propagation of calcium signals in this model in presence and absence of external stimulus that corresponds to moving target in real world. We also do comprehensive parametric study of our model outlining how and why it behaves with different values of parameters and thus characterizing the facilitation mechanism.

# 5. RESPONSE FACILITATION:

## *5.1. Response Facilitation:*

*Facilitation* is an increase in excitability of an STMD neuron, dependent upon ongoing excitation by a small-target stimulus. It is not strictly a function of how long an STMD neuron is excited by small targets; rather, its effect is most pronounced when a target moves along a *continuous path* in the visual field 48]. This is a constraint that must be obeyed by the images of real, physical targets – except for periods when they may be occluded by intervening objects. Therefore, we can think of *facilitation* as a means to exploit a natural constraint in order to gain confidence in the target detection mechanism in the actual presence of a target. For the noisy and low-amplitude visual signals that are evoked by small targets, this may give a significant boost to the reliability of detection.

## *5.2. Experiments for Response Facilitation:*

A variety of experiments have been conducted to characterize the process of facilitation. These experiments have been conducted with immobilized insects viewing a screen on which moving small-target stimuli are presented. By analyzing experiments involving intercellular recordings from individual STMD neurons and the sensitivity of the STMDs to small target contrast, Wiederman and O'Carroll and their labs have shown that facilitation corresponds to a modulation of contrast gain in the neural pathway leading to the STMDs.

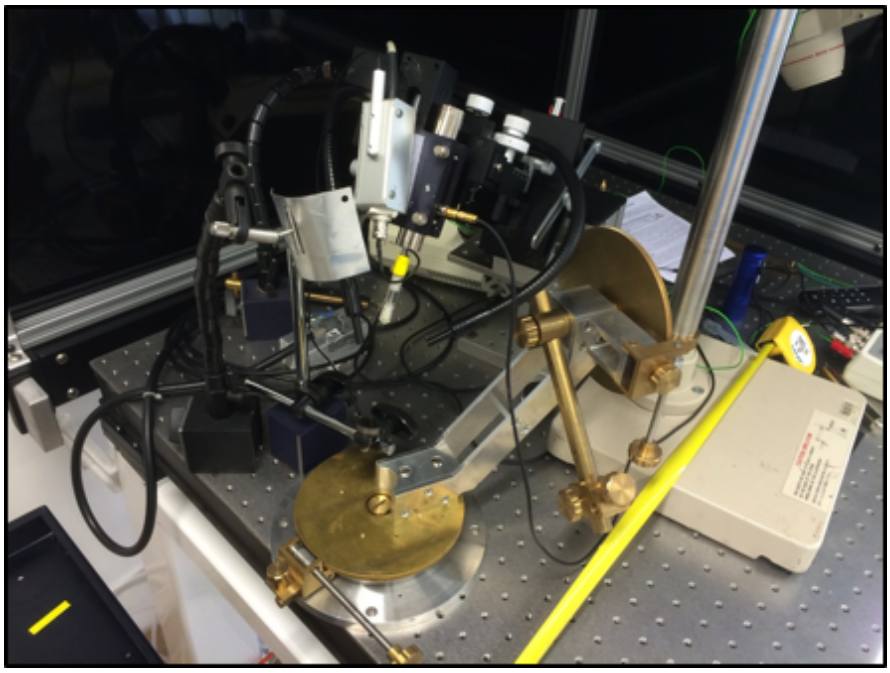

*Figure 1: Picture of Electrophysiology Station for conducting Facilitation experiments in dragonflies. The insect (dragonfly) is mounted at center and the display screen is at front left. Image courtesy: David O'Carroll (Lund University).*

In a critical subset of these experiments, the insects have been subjected to a priming target that moves part way through the receptive field of the STMD and then vanishes, followed by a probe stimulus consisting of a target moving briefly along a short path at some other location. By repeating this sequence for various probe locations, and recording the neural responses, a spatial map of the responsiveness of the STMD following the priming stimulus can be assembled. When this is compared to responsiveness map built without a primer, the degree of facilitation of the neuron due to the primer can be assessed as a function of position in the visual field.

*5.3. Predictive nature of Facilitation:*

Comparing maps of the receptive field in facilitated and unfacilitated states, it can be seen that the region of facilitation is limited in size and appears at and in front of the last position of the priming stimulus. Moreover, when there is a delay between the primer and the probe stimuli, it can be seen that the region of facilitation has actually propagated through space in the direction in which the target was moving. These results clearly show that facilitation can be regarded as predictive in nature. Facilitation that doesn't propagate on its own could still translate as a result of the fact that it is evoked by a moving stimulus, but in that case, the facilitation would not keep moving after the stimulus ceases.

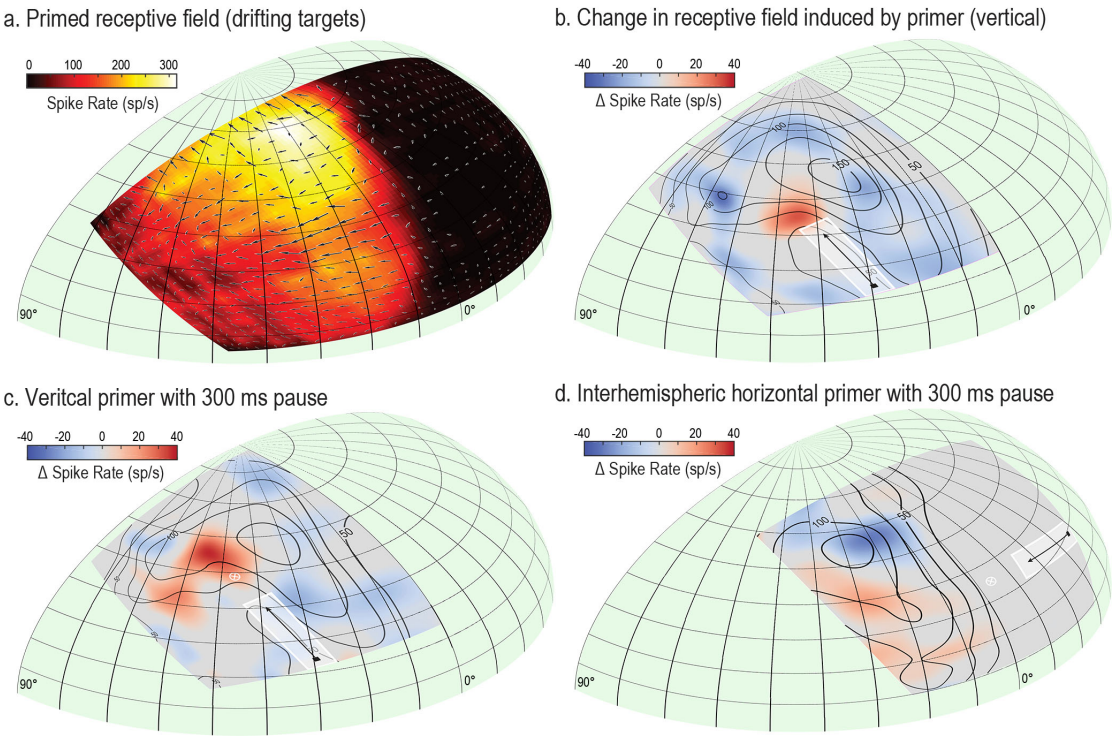


*Figure 2: A predictive focus facilitates responses to a moving target. Map of facilitation for a priming stimulus consisting of a small target drifted upward partway through the receptive field of identified neuron CSTMD1. The graphics depict a projection onto the upper front quarter of the visual field. The path of the primer is indicated by a vertical black arrow at lower center. Degree of facilitation (change in spike rate in response to probe) is color coded, with warm colors indicating enhanced responsiveness, and cool colors depressed. Panel a depicts the baseline receptive field sensitivity of the neuron, and b depicts the change in sensitivity induced by the primer, when the probe stimuli immediate follow it. In c and d, there is a pause between the end of primer motion and the imposition of the probe stimuli. Image courtesy: David O'Carroll (Lund University) and Steven Wiederman (University of Adelaide).*

### *5.4. Inter-hemispherical transfer of facilitation:*

If we look at panel d of Figure 2, we can see this (monocular) neuron, which only gets input from one eye has responses only in right hemisphere of brain, whereas stimulus is moving in the left hemisphere. So, somehow there is transmission of facilitation all the way across the brain. There might be a dedicated neuron that goes over the other side of the brain and stimulates the facilitatory network. This shows that some degree of facilitation can be transmitted from one side of the brain to other side.

## 6. ANATOMY AND PHISOLOGY OF STMD SYSTEMES

There are two classes of STMDs, defined by their receptive field extents: wide-field STMDs and small-field STMDs. The STMD cells reside in the third optic ganglion, the lobula, as shown in Figure 3. There is evidence suggesting that the small-field STMDs, which are located more peripherally than the wide-field STMDs, project their outputs to the wide-field cells. It is not entirely certain at present where the facilitation phenomenon takes place: there is evidence that small-field STMDs, which arborize in the primary lobula and are organized retinotopically, may be subject to facilitation [12] and the locus of the facilitatory 'hot spot' is (perhaps not

coincidentally) roughly the same size as the receptive fields of small-field STMDs. However, it cannot be ruled out that the moving facilitation takes place where dendritic arborizations of wide-field STMDs occur, such as the medial lobula and other areas deeper in the ganglion. For example, it is plausible that a facilitatory network(s) residing in these regions is stimulated by the small-field inputs that converge on the wide-field STMDs, but then exerts its action on the dendrites of the wide-field neurons themselves.

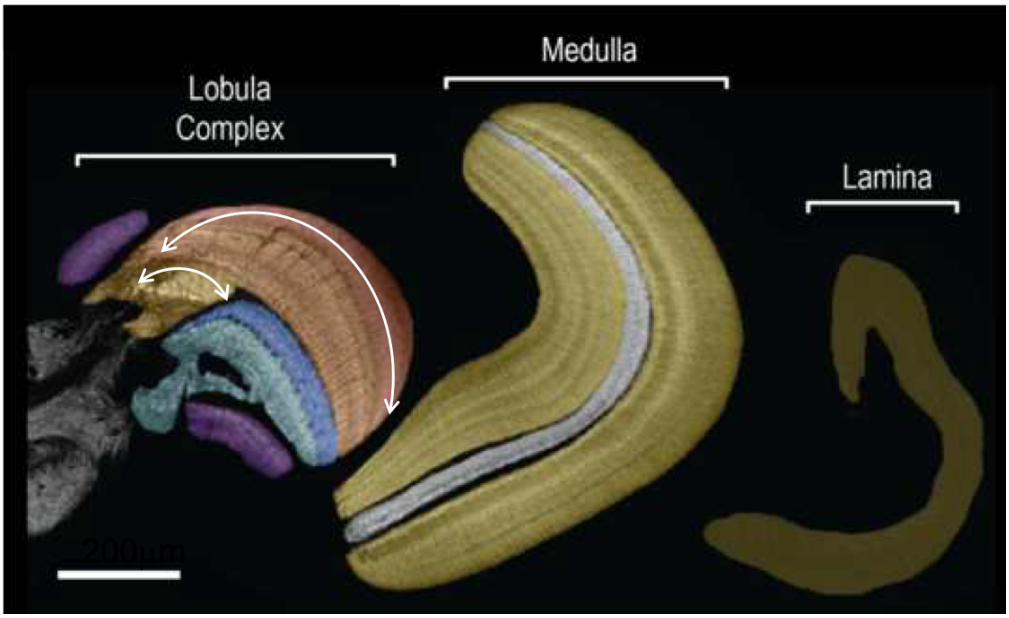


*Figure 3: EMBARGOED Horizontal section of the optic ganglia of the dragonfly Hemicordulia tau. This image is for the right eye, and depicts the first optic ganglion (the lamina), the second (the medulla), and the third (the lobula complex, at left). The primary lobula, shown in pink, is where small-field STMDs receive their inputs, whereas wide-field STMDs arborize elsewhere, including in the medial lobula, the smaller tan structure below the left part of the primary lobula. Image courtesy of J. Fabian, B. el Jundi, S. Wiederman, and D. O'Carroll. Release of this figure is embargoed pending publication by its authors.*

It is observed that the region of facilitation moves at a rate of 30-40 degrees/sec in the visual field [12], which in turn dictates the range of speeds that must be assumed by a propagating signal that mediates the facilitatory process in retinotopic areas of the brain. The outer layers of the primary lobula as seen in Figure 3 span about 750µm in horizontal section, corresponding to roughly 135° subtense in visual space; this implies that a moving facilitatory signal in this neuropil would have to propagate at ~170µm/s to 220µm/s. Conversely, the medial lobula (also shown in Figure 3), where some wide-field STMDs arborize, is around 1/4 to 1/5 of this size. It is not entirely certain how this structure, or the dendrites of wide-field STMDs in general, scale relative to the visual space they service, but it *is* clear that required propagation speeds would be smaller, on the order of tens of µm/s, if propagating facilitation takes place there.

# 7. PROBLEM STATEMENT

Because studies [12] have shown that locus of facilitation induced by a moving target propagates in visual space even after a small target stimulus ceases, we are proposing that it could be supported by traveling wave phenomena in retinotopically-organized regions of the visual system.

We hypothesize that there are some auxiliary layers or two dimensional networks of cells that interact with STMDs; these are stimulated in some way by STMDs. This stimulus propagates through the network which can account for propagation of facilitation in space, and then the network interacts reciprocally with STMDs, increasing their excitability. This traveling wave (or propagating facilitation) is *reinforced* as a result of a traveling stimulus.

As discussed above, there is a specific speed (range) with which facilitation propagates in the structures in which such a network could reside; therefore we can say speed is an important constraint. Electrical signals in neurons are a logical possibility to represent facilitation, but these propagate at speeds that are far too great. So, our motivation is to choose models that that allow slower wave propagation, and we have identified calcium waves as a plausible candidate. In this thesis, we model calcium waves in two media: a) an interconnected network of astrocytes, and b) an interconnected network of neurons.

# 8. MECHANISM FOR FACILITATION

In this section, we consider the likely features of a biologically-plausible mechanism for predictive facilitation.

## *8.1. Network of Cells:*

Facilitation as a mechanism is spatially local, but it may possibly be universal in the wide-field STMDs. But it has been only been confirmed experimentally in 2-3 identified neurons (mainly due to the difficulty of identifying and recording from such cells) and thus many neurons might be involved in the computation of facilitation over a broad region. Thus we assume that it is supported by a network of cells that forms a heavily-interconnected, two-dimensional layer or web with many randomly-oriented processes and interconnections between these cells, through which a facilitatory signal can propagate in a roughly isotropic fashion. This facilitatory signal would be evoked by activity in STMD neurons, and in turn it affects the excitability of STMD neurons or neural processes with which it interacts.

## *8.2. Regenerative Mechanism:*

The active wave propagation, whether chemical or electrical, requires a regenerative mechanism in order to take place. This regenerative mechanism would involve some form of positive feedback. In any such mechanism, propagating signal causes changes in the cell membrane, like opening of ion channels that further reinforces the signal by influx of more ions that increases signal strength.

## *8.3. Propagation speed:*

Signal that propagates in such a network needs to have a propagation speed less than a mm/s, as discussed above. Membrane potentials in cable-like cellular structures are far too fast for our purpose as they have propagation speed on the order of cm/s or more.

### *8.4. Calcium waves as a mechanism for facilitation*

Calcium signaling in recent time has gained lot of attention and recent work suggests that calcium signaling could play a crucial role in the nervous system. Since calcium signals propagate considerably more slowly than electrical potentials in cells, we propose that propagating calcium waves could be a potential mechanism for facilitation. Also, calcium signaling is present in many kinds of cells including neurons and astrocytes.

## 9. BACKGROUND

Calcium waves are seen in both glia cells and neurons, and since we are considering both the cells as possible building block for our models, so in this section we will give brief background about neurons and glia cells and how calcium signals are triggered and transmitted in them.

### *9.1. Glial Cells:*

Glial cells or simply glia were discovered in 1856 by the pathologist Rudolf Virchow in his search for a "connective tissue" in the brain. Glial cells, also called as Neuroglia, are non-neuronal cells that plays a very crucial role in central and peripheral nervous system. The term "Glia" comes from the Greek and implies these cells are the "glue" of the nervous system. They initially got this name, because they seem to fill spaces between neurons to hold them together.

There are different types of glial cells in the central nervous system. Glial cells include oligodendrocytes, astrocytes, ependymal cells and microglia, and in the peripheral nervous system glial cells include Schwann cells and satellite cells.

For over a century, it was believed that the glia did not play any role in neural signal processing. However, with improved techniques, researchers have found out that glia cells do have an important role to play in assisting/ supporting the neurons to form synaptic connections between each other or possibly between neurons and glia cells themselves.

Out of different types of glial cells, the most abundant type of cells in the vertebrate central nervous system are Astrocytes. They constitute up to 40% of all glia cells. Astrocytes are star shaped glia cells and are found in proximity to neurons. Astrocyte-like glial cells are also found in the nervous systems of insects [26].

Astrocytes are non-electrically excitable, unlike neurons. However, they do display a form of excitation that is based on variation of $Ca^{2+}$ concentration in cytosol. Localized changes (increase or decrease) in concentration of $Ca^{2+}$ can propagate in the form of a wave like pattern, which is called calcium wave. In last decade, studies and research in vertebrates has shown that astrocytes propagate intra- and intercellular calcium waves in response to stimulation. The waves could be transmitted over tens of μm because of regenerative mechanisms that are present in astrocytes.

### *9.2. Neurons:*

A neuron, also known as a nerve cell, is an electrically excitable cell that communicates with other cells via specialized connections called synapse. It is the primary component of nervous system, along with the glial cells. Neurons are typically classified into three types based on their function. Sensory neurons respond to stimuli such as touch, sound, or light that affects the cells of the

sensory organs. Motor neurons send signals from brain and spinal cord to control effectors such as muscles. Interneurons connects neurons to other neurons within the same region of the brain.

Most neurons consist of three parts: a cell body, dendrites, and a single axon. The cell body is usually compact and axon and dendrites are filaments that extrude from it. Dendrites are usually tens to a few hundred micrometers in length and axon can be as long as 1 meter in humans and other vertebrate species. The function of the axon is usually regarded as transmitting the neural output over some distance to other, target neurons. However, many interneurons that process signals locally do not have clearly defined axons. We model a neural network for facilitation that is composed of such neurons.

The signaling process in neurons is partly electrical and partly chemical. Neurons are normally polarized to a negative potential with respect to the extracellular space; the signaling potentials are typically depolarizing if they are excitatory. However, some inputs can generate hyperpolarization too. Once a neuron has been stimulated by some sort of stimulus, it generates an electric potential that can travel through the length of the cell. This is 'electro' part of the electrochemical. Axons typically transmit active electrical signals called action potentials. Once the electric signal reaches the axon terminal at the end of the cell, or in some cases the dendrites, it triggers the release of certain chemical messengers, also known as neurotransmitters. This is 'chemical' part of electrochemical. These neurotransmitters allow one neuron to communicate with another.

Calcium ($Ca^{2+}$) is a ubiquitous second messenger for many physiological roles. It is of critical importance to neurons, as it governs the release of neurotransmitters and thus helps in the transmission of signals between neurons [4].

### *9.3. Ca Signaling/ Wave:*

A calcium wave is defined as a moving, localized increase in cytosolic $Ca^{2+}$, which in many vertebrate neurons and astrocytes may be followed by a succession of similar events in a periodic wave-like fashion. These Ca waves can be restricted to one cell (intracellular) or transmitted to neighboring cells (intercellular). The cellular and molecular mechanism involved in the triggering and transmission of $Ca^{2+}$ are well studied and researched. In this section, we will give background about mechanisms involved in triggering and transmission of $Ca^{2+}$ waves in astrocytes and neurons.

#### 9.3.1. *Triggering Calcium Waves in Astrocytes:*

The basic mechanism that lead to intracellular $Ca^{2+}$ waves in astrocytes usually involve the release of neurotransmitters onto the astrocytes which leads to a chain of reactions in the following order: activation of G-protein-coupled receptors, activation of phospholipase C, and the production of Inositol trisphosphate ($IP_3$), which following Inositol trisphosphate receptor ($IP_3R$) activation leads to $Ca^{2+}$ release from the endoplasmic reticulum (ER) [19, 11]. These $Ca^{2+}$ waves are spatially and temporally complex events involving many $Ca^{2+}$ release sites (receptor channels), which then propagate throughout the cell by amplification mechanism. This amplification mechanism consists of four components, two of which are positive and negative feedback mechanism each. Once triggered, intracellular $Ca^{2+}$ waves can be transmitted to neighboring cells.

*9.3.2. Triggering Calcium Waves in Neurons:*

Like astrocytes, some neurons may also have $Ca^{2+}$ waves, which use both extracellular and intracellular sources of calcium for triggering and transmission. The mechanisms responsible for regulating the influx of external calcium are well established [20]. Voltage-operated calcium channels are used to trigger the release of neurotransmitter at synaptic junctions, and they contribute to dendritic action potentials. In addition, neurotransmitters can induce an influx of calcium (as well as other ionic species) using receptor-operated channels located primarily at postsynaptic sites. The N-methyl-D-aspartate (NMDA) receptor, which is activated by the neurotransmitter glutamate, is one class of receptor whose channels conduct a significant proportion of calcium ions. As far as intracellular calcium is concerned, two receptors, InP3 receptors or Ryanodine receptors (RYRs) are responsible for releasing $Ca^{2+}$ from internal stores. The endoplasmic reticulum contributes to the dynamics of $Ca^{2+}$ signaling by acting either as a source or a sink of $Ca^{2+}$.

*9.4. Transmission of Ca waves:*

The law governing lateral $Ca^{2+}$ transport within a neuron/ astrocyte is provided by the diffusion equation. (Laterally-diffusing $Ca^{2+}$ in turn can mediate the influx of additional calcium through adjacent areas of cell membranes by the mechanisms discussed above – these are the active mechanism of calcium waves.) Therefore, the propagation of intracellular $Ca^{2+}$ waves is affected by the diffusion coefficient of $Ca^{2+}$ ions in cytosol.

The transmission of Ca waves between cells can take place through two pathways. First is direct communication between cytosol of two adjoining cells through “gap junction” channels. Gap junctions are a specialized intercellular connection between two cells. They directly connect the cytoplasm of two cells, which allows various molecules and ions to directly pass through a regulated gate between cells.

Another type of pathway is via indirect communication, where there is no physical connection between the cytoplasm in two cells. This type of communication depends upon the release of gliotransmitters that activates membrane receptors on neighbor cells. Once membrane receptors are activated, these cells respond with increase in intercellular $Ca^{2+}$ elevations. Gliotransmitter are chemicals released from glia cells that facilitate neuronal communication between neurons and other glia cells, and this communication may be triggered through calcium waves/ signals.

These waves propagating between different cells are called Intracellular calcium waves (ICWs). ICWs are spatially and temporally complex events involving the recruitment of elementary $Ca^{2+}$ release sites, which then propagate through cell by feedback mechanism.

## 10. MODELS FOR PROPAGATION

In the project supporting this MS research, we propose three candidates for biophysically-plausible substrates to model propagating facilitation: 1) a network of glial cells in which the signal is carried by calcium ions, with lateral transport by diffusion, and waves that are propagated with a regenerative positive feedback mechanism; 2) a network of neurons in which the signal is similarly carried by calcium ions, with similar wave-like propagation; and 3) a network of small neurons in which propagating electrical signals are delayed frequently by the presence of excitatory synapses

with slow kinetics. This MS project is focused on the first and second candidate mechanism, and based on modeling 1) cellular processes, or "dendrites, and 2) networks of cells, in which calcium waves are the primary signaling mechanism.

*10.1. Lateral calcium transport by diffusion in a dendrite:*

Calcium waves propagate laterally in astrocytes and neurons by diffusion. We model the lateral transport of calcium during the propagation of calcium waves in one-dimensional cellular processes (dendrites) using a one-dimensional version of Fick's law (the diffusion equation), which can be represented as:

$$\frac{\partial}{\partial t}[Ca^{2+}] = D_{Ca}\frac{\partial}{\partial x^2}[Ca^{2+}] + j_{ca} \qquad 1$$

where, $[Ca^{2+}]$ is concentration of calcium ions, $\frac{\partial}{\partial t}[Ca^{2+}]$ is the local time rate of change in calcium ion concentration, and $D_{Ca}$ is Ca diffusion coefficient. $j_{ca}$ is influx of calcium ions in every compartment due to the action of pumps and receptor channels, as described in section 7.2.

10.2. *Model for calcium dynamics in astrocytes:*

In the following section we introduce our models for calcium transport mechanism, pumps, different chemical reactions and components that contribute to $j_{Ca}$ our astrocytes model. Most of the model components discussed in below sections have rate constants associated with them which are scaled by a time increment $\Delta t$ for purposes of temporal integration.

In our astrocyte model, we are not distinguishing the Endoplasmic reticulum (ER) and extra-cellular space, we just call them as stores of calcium and they are assumed to have high concentration of calcium as compared to cytosolic calcium concentration present inside the cell. And, the small influx of calcium that we get into cytosol is assumed not to change the difference. So, this difference between two concentrations is also assumed to be constant.

*10.2.1. Trans-membrane calcium transport model for astrocytes:*

Figure 4 shows the complete trans-membrane calcium dynamics model for astrocytes in our model, in quasi-kinetic form. We also include calcium buffering by Calbindin in this diagram, since like the transmembrane calcium fluxes, it is computed locally. The positive feedback loop for calcium entry into the cytosol can be described as follows: Neural input (presumably glutamate release) opens calcium channels; the influx of calcium triggers the cleaving of InP3 from DAG; InP3 activates InP3 receptors, leading to the influx of more calcium; the positive-feedback episode is terminated by reduction of open probability of the InP3 receptor, which reduces the loop gain to less than unity.

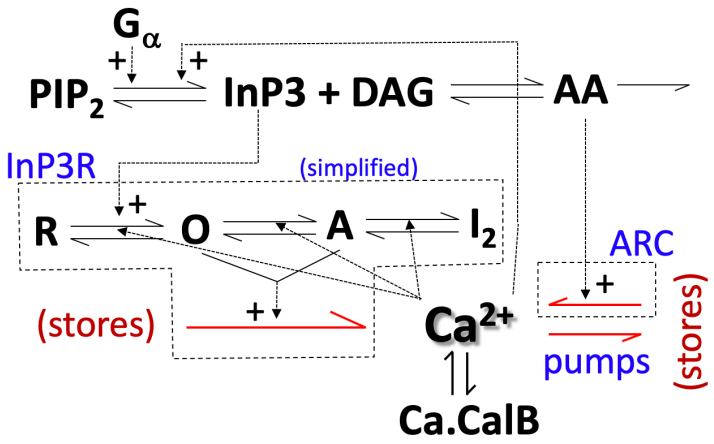


*Figure 4: Trans-membrane calcium transport model for astrocytes. The buffering action of Calbindin (CalB) is also included for completeness, since like membrane transport it is modeled locally in space. ⇌ (in black color) represents reversible reactions and ⇌ (in red color) represents flow of calcium in and out of $Ca^{2+}$ stores. Dotted lines and arrows represents influence of a given molecule/chemical on a reaction; and a + sign represents a positive influence on that reaction. InP3R indicates the InP3 receptor, and R, O, A and $I_2$ are different states for this receptor's calcium channels; ARC represent Arachidonate-regulated calcium channels. Figure courtesy of Patrick Shoemaker.*

The Arachidonate-regulated calcium (ARC) channels have high $Ca^{2+}$ selectivity and are activated by Arachidonic acid (AA). ARC channels are the source of initial calcium entry into the cytosol from stores. And, calcium pumps like (SERCA pumps; introduced below) and other sequestration mechanisms are responsible for removing calcium from the cytosol. As the $Ca^{2+}$ diffuses in the cytosol, it can encounter high-affinity $Ca^{2+}$-binding proteins / substances, such as Calbindin-$D_{28k}$ (CalB) that act as cytosolic $Ca^{2+}$ buffers. These $Ca^{2+}$-buffers act as modulators of short-lived intracellular $Ca^{2+}$ signals; they affect both the temporal and spatial aspects of these transient increases in $Ca^{2+}$.

10.2.2. *InP3 receptor kinetics:*

The InP3 receptors that mediate positive feedback are critical for calcium wave propagation. Their properties are quite complex (in fact, they have been characterized as 'bizarre' in reviews (Dawson, 1997)). We have chosen to implement a model for the receptor kinetics that derives from a 10-state model that collapses into 6 states with the introduction of state-dependent rate functions [15].

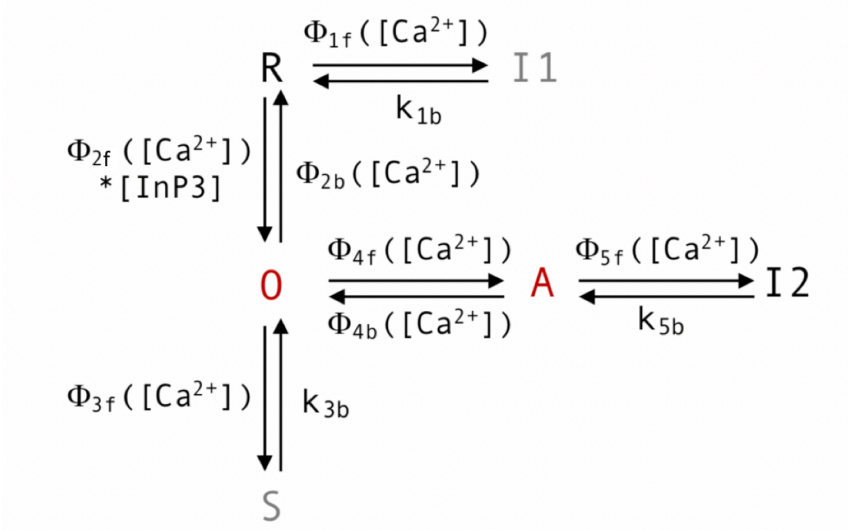


*Figure 5: The Sneyd-Dufour model for InP3 receptor kinetics. Opening of the receptor's calcium channel is associated with states O and A. The functions denoted by $\phi$ are calcium-dependent rate functions. Transition from the native state R to O involves binding of the ligand InP3, reflected by its presence as a factor in the rate for that transition. The states rendered in gray, I1 and S, were found to have little participation in receptor function under the conditions we simulated, and are not included in our models. This kinetic structure is associated with each of four subunits of the complete receptor.*

The states rendered in gray, I1 and S (in Figure 5), were found to have little participation in receptor function under the conditions we simulated, and are not included in our models. In terms of channel open probability, the state O corresponds to 'weakly open' and A to 'strongly open'. The kinetics in Figure 5 apply to each of four subunits that make up the complete receptor; the total open probability is thus $(0.1 * O + 0.9 * A)^4$. When InP3 concentration is stepped, the time-course of the distribution of the subunits among the states leads to a brief period of high open probability followed by much lower open probability. This feature is essential to the formation of calcium waves in cells incorporating the InP3 receptor.

The calcium influx through InP3 receptor channels is given by an expression of the form:

$$j_{InP3} = k_{Ca} * Open_{InP3} \quad (2)$$

where, $k_{Ca}$ is the calcium influx rate constant for open InP3 channels, and is proportional to the InP3 receptor density in the ER and/or plasma membranes. $Open_{InP3}$ is probability of open states in InP3 channels. $Open_{InP3}$ is modeled according to below] and can be calculated as the sum of the two open states, $O$ and $A$ in the system of ordinary differential equations (given below).

$$Open_{InP3} = (f_O * O + f_A * A)^4 \quad (3)$$

where, $f_O$ *and* $f_A$ are relative dependence of open probability on O and A states.

The InP3 channels states are calculated as follows;

$$r_{O\to R} = \phi_{2ba}\,([Ca^{2+}])$$

$$r_{R\to O} = \phi_{2fa}([Ca^{2+}] * [InP_3])$$

$$r_{O\to A} = \phi_{4fa}([Ca^{2+}])$$

$$r_{A\to O} = \phi_{4ba}([Ca^{2+}])$$

$$r_{A\to I_2} = \phi_{5fa}([Ca^{2+}])$$

$$r_{I_2\to A} = r_{5b}$$

$$\frac{dR}{dt} = (r_{O\to R} * O) - (r_{R\to O} * R)$$

$$\frac{dO}{dt} = (r_{R\to O} * R) + (r_{A\to O} * A) - ((r_{O\to R} * O) + (r_{O\to A} * O))$$

$$\frac{dA}{dt} = (r_{O\to A} * O) + (r_{I_2\to A} * I_2) - \left((r_{A\to O} * A) + (r_{A\to I_2} * A)\right)$$

$$\frac{dI_2}{dt} = \left(r_{A\to I_2} * \mathrm{A}\right) - (r_{I_2\to A} * \mathrm{I}_2)$$

where $r_{5b}, \phi_{2ba}, \phi_{2fa}, \phi_{4fa}, \phi_{4ba}, \phi_{5fa}$ are InP3 receptor states rate functions of calcium concentration $[Ca^{2+}]$ as shown in Figure 5. We compute these functions using equations shown below, where Ca is calcium concentration in uM and other rate and channel constant values are taken from Table 1.

$$\phi_{1fA} = \frac{(k1f * L1 + l2f)}{L1 + \left(1 + \frac{L1}{L3}\right)} * Ca \quad (4)$$

$$\phi_{2fA} = \frac{(k2f * L3 + l4f * Ca)}{L3 + \left(1 + \frac{L1}{L3}\right)} * Ca \quad (5)$$

$$\phi_{2bA} = \frac{(k2b + l4b * Ca)}{\left(1 + \frac{Ca}{L5}\right)} \quad (6)$$

$$\phi_{3fA} = \frac{(k3f * L5)}{(L5 + Ca)} \quad (7)$$

$$\phi_{4fA} = \frac{(k3f * L5 + l6f) * Ca}{(L5 + Ca)} \quad 8$$

$$\phi_{4bA} = \frac{(k4b + l6b) * L1}{(L1 + Ca)} \quad 9$$

$$\phi_{5bA} = \frac{(k1f * L1 + l2f) * Ca}{(L1 + Ca)} \quad 10$$

*10.2.3. Models for PIP2 – InP3 – DAG – AA Signaling Cascade:*

Binding of a signaling molecule to a G protein-coupled receptor (GPCR) results in G protein activation, which in turn triggers the production of second messengers. The effector enzymes in this cascade is Phospholipase C (PLC). This PLC cleaves Phosphatidylinositol 4,5-bisphosphate (PIP2) into IP3 (inositol triphosphate) and DAG (diacylglycerol). IP3 diffuses over to ER (Endoplasmic Reticulum) and it binds with calcium ion channel and it allows calcium ions ($Ca^{2+}$) to flow from inside of the ER to the cytosol. And some of the DAG along with $Ca^{2+}$ ions works together to activate PKC, which adds phosphates to target protein which triggers the cellular response. Also, studies of the DAG/protein kinase C (PKC) pathway indicate that PKC is involved in the termination of astrocytic $Ca^{2+}$ transients [23, 24, 25]. Equations given below show clearly that PKC has an inhibitory effect on InP3 production – but we found when looking at the experimental results that this effect is minimal, so we left it out of the Figure 4.

Accordingly, equations for InP3, AA and PKCv updates are as following:

$$\frac{dInP_3}{dt} = \frac{G_{in} + kd_{1f} * Ca}{1 + k_{i2} * PKC_v} - k_{1b} * InP_3 \quad 11$$

$$\frac{dAA}{dt} = k_{1b} * InP_3 - k_{1b} * AA \quad 12$$

$$\frac{dPKC_v}{dt} = k_{4f} * Ca * (PKC_0 - PKC_v) - k_{4b} * PKC_v \quad 13$$

where parameters and rate constants used are defined in the Table 1 and $G_{in}$ represents the local concentration of G-protein.

*10.2.4. Models for Pumps:*

The models for pumps are taken from [14] and are adapted to account for efflux from plasma membrane pumps (PMCA and NCX pumps), which are seen in Glia cells [22]. The calcium flow associated with pumps is described by a combination of first order Hill's equation that corresponds

to plasma membrane pumps and second order Hill's equation that corresponds to SERCA pumps, respectively.

$$j_{pumps} = k_p^1 * \left(\frac{C_s}{\left(k_{pc}^1 + C_s\right)}\right) + k_p^2 * \left(\frac{C_s^2}{\left(k_{pc}^2 + C_s^2\right)}\right) \quad 14$$

where $k_p^1$ , $k_{p,}^2$ $k_{pc}^1$ and $k_{pc}^2$ are calcium 1st- and 2nd-order pump constants, $C_s$ is cytosolic calcium concentration, and $j_{pumps}$ is calcium efflux due to pumps.

*10.2.5. Model for Ca Buffering:*

Calcium buffering can be described as an *"uptake and release"* of free calcium in cytosol by $Ca^{2+}$-binding proteins (e.g., Calbindin-$D_{28k}$). We elected to model all such buffering by a single reaction. This mechanism is described as a reversible reaction given by:

$$Ca^{2+} + CalB \leftrightharpoons Ca.CalB$$

As the $Ca^{2+}$ diffuses in the cytosol, free $Ca^{2+}$ binds (reacts) with CalB, that acts as cytosolic $Ca^{2+}$-buffers. This bounded $Ca^{2+}$ is released back into cytosol by the reverse reaction.

The equations for calbindin and cytosolic calcium are given by:

$$j_{s_{fb}} = k_{c_{bf}} * C_s * (CalB0 - [Ca.CalB]) \quad 15$$

$$j_{s_{bf}} = k_{c_{bb}} * [Ca.CalB] \quad 16$$

$$\frac{dC_s}{dt} = j_{s_{bf}} - j_{s_{fb}} \quad 17$$

$$\frac{d[Ca.CalB]}{dt} = j_{s_{fb}} - j_{s_{bf}} \quad 18$$

where $k_{c_{bf}}$and $k_{c_{bb}}$are rates for calcium buffering, with baseline calbindin being, CalB0 = 40 μM. $C_s$ and $[Ca.CalB]$ is cytosolic and bounded calcium concentration, respectively. Here we use "flux" symbols $j_{s_{bf}} and\ j_{s_{fb}}$ for rates of change in unbound and bound calcium concentrations, respectively, for consistency with the kinetic formalism.

*10.2.6. Model for Gap Junctions:*

Gap junctions are a specialized intercellular connection between cells (either astrocytes or neurons). They directly connect the cytoplasm of two cells, which allows various molecules, ions and electrical impulses to directly pass through a regulated gate between cells. In vertebrate astrocytes, evidence suggests that there is direct exchange of InP3 and $Ca^{2+}$ through gap junction-like interconnections between cells. But as per [18], calcium flow through gap junctions seems to be extremely limited, so we are ignoring it in our model and thus we only model the direct exchange of InP3.

The influx or efflux of InP3 through gap junctions is modeled by the following equation:

$$j_{Gap} = r_{inp3} * ([InP3_{c1}] - [InP3_{c2}]) \quad 19$$

where $r_{inp3}$ is the rate constant for flow of calcium between cells through gap junctions and $j_{Gap}$ is the flow of InP3 from cell 1 into cell 2, and this is positive if concentration is higher in cell 1, and negative if concentration is higher in cell 2.

*10.2.7. Model for leakage:*

The influx of calcium per unit area of plasma membrane due to leakage mechanism is assumed to be constant, because the difference in calcium concentration between cytosolic and external calcium is assumed to be nearly constant, due to the much higher calcium levels in the external space. Leakage flux is given by following equation:

$$j_{leakage} = k_{lk} \quad 20$$

where $k_{lk}$ is calcium leakage rate in uM/S.

*10.2.8. Model for ARC Channels:*

Unlike store-operated channels (activation of which is, dependent on the depletion of internal $Ca^{2+}$ stores, notably the endoplasmic reticulum (ER)), Arachidonate-regulated $Ca^{2+}$ (ARC) channels specifically depend on the receptor-mediated generation of low levels of intracellular arachidonic acid [21].

In our model, ARC channels are only responsible for initial influx flow of calcium. The calcium influx through ARC channels is given by following equations:

$$j_{ARC} = k_{aa} * AA \quad 21$$

where $k_{aa}$ is the calcium influx rate for open ARC channels and AA is concentration of arachidonic acid.

| Parameter / Constant | Nominal Value | Units | Definition |
|---|---|---|---|
| *DCa* | 240 | $\mu m^2.s^{-1}$ | Ca diffusion coefficient in astrocytes |
| *fCa* | 0.3 | - | fraction to reduce DCa due to intracellular crowding |
| *DInP3* | 300 | $\mu m^2.s^{-1}$ | InP3 diffusion coefficient in astrocytes |
| *fInP3* | 0.7 | - | fraction to reduce DInP3 due to intracellular crowding |
| *kGI* | 40 | $\mu m.s^{-1}$ | Rate of InP3 production induced by glutamatergic input |
| *kd1f* | 6 | $\mu m.s^{-1}$ | Rate constant for [Ca]-dependent production of $InP_3$ |
| *kcbf* | 0.7 | $\mu m^{-1}.s^{-1}$ | Rates for calcium buffering |
| *kcbb* | 10 | $s^{-1}$ | Rates for calcium buffering |

| | | | |
|---|---|---|---|
| *kCa* | 600 | $\mu m.s^{-1}$ | Calcium influx rate constant for open InP3R channels |
| *kaa* | 6 | $\mu m^2.s^{-1}$ | Calcium influx rate for open ARC channels |
| *kGI* | 40 | $\mu m.s^{-1}$ | rate of InP3 production induced by glutamatergic input |
| *rinp3* | 500 | $\mu m.s^{-1}$ | Rate constants at interconnections/ gap junctions |
| *ki2* | 0.0943 | $\mu m^{-1}$ | for inhibition of InP3 production by PKC |
| *k4f* | 0.6 | $\mu m^{-1}.s^{-1}$ | Rate constant for activation of PKC |
| *k4b* | 0.5 | $s^{-1}$ | Rate constant for deactivation of PKC |
| $PKC_0$ | 1 | $\mu m$ | Available concentration of PKC |
| *kp1* | 75 | $\mu m.s^{-1}$ | Calcium 1st-order pump constants |
| *kp1c* | 1.8 | $\mu m$ | Calcium 1st-order pump constants |
| *kp2* | 12 | $\mu m.s^{-1}$ | Calcium 2nd-order pump constants |
| *kp2c* | 0.10 | $\mu m$ | Calcium 2nd-order pump constants |
| *K1k* | 1 | $\mu m.s^{-1}$ | Calcium leakage rate |
| *k1b* | 2.5 | $\mu m.s^{-1}$ | for conversion of InP3 into AA (and then back into PIP2) |
| *k1f* | 0.640 | $\mu m^{-1}.s^{-1}$ | constant associated InP3R rate functions |
| *k1b* | 0.040 | $s^{-1}$ | constant associated InP3R rate functions |
| *k2f* | 37.40 | $\mu m^{-1}.s^{-1}$ | constant associated InP3R rate functions |
| *k2b* | 1.400 | $s^{-1}$ | constant associated InP3R rate functions |
| *k3f* | 0.110 | $s^{-1}$ | constant associated InP3R rate functions |
| *k3b* | 29.80 | $s^{-1}$ | constant associated InP3R rate functions |
| *k4f* | 4.000 | $\mu m^{-1}.s^{-1}$ | constant associated InP3R rate functions |
| *k4b* | 0.540 | $s^{-1}$ | constant associated InP3R rate functions |
| *L1* | 0.120 | $\mu m$ | constant associated InP3R rate functions |
| *L3* | 0.025 | $\mu m$ | constant associated InP3R rate functions |
| *L5* | 57.40 | $\mu m$ | constant associated InP3R rate functions |
| *l2f* | 1.700 | $s^{-1}$ | constant associated InP3R rate functions |
| *l2b* | 0.800 | $s^{-1}$ | constant associated InP3R rate functions |
| *l4f* | 1.700 | $\mu m^{-1}.s^{-1}$ | constant associated InP3R rate functions |
| *l4b* | 2.500 | $s^{-1}$ | constant associated InP3R rate functions |
| *l6f* | 4707 | $s^{-1}$ | constant associated InP3R rate functions |
| *l6b* | 11.40 | $s^{-1}$ | constant associated InP3R rate functions |
| *r1b* | 0.840 | $s^{-1}$ | Rate constants associated with the state-dependent InP3R model |
| *r3b* | 29.80 | $s^{-1}$ | Rate constants associated with the state-dependent InP3R model |
| *r5b* | 0.840 | $s^{-1}$ | Rate constants associated with the state-dependent InP3R model |

*Table 1: List of parameters and constants associated with Astrocyte Model. Parameters that are shown in red color are varied experimentally in our experiments, while others are fixed at give values. '-' in units column represents unitless parameter value. All parameters and constants associated with InP3 rate functions are referred from [15].*

*10.3. Models for calcium dynamics in neurons:*

In the following section, we introduce calcium transport model for neurons, which includes RyR channels, and different calcium pumps.

*10.3.1. Trans-membrane calcium transport model for neurons:*

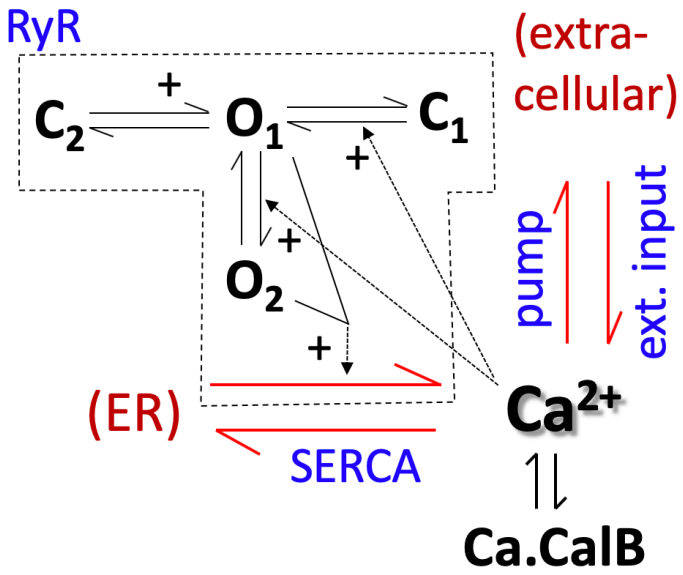


*Figure 6: Trans-membrane calcium transport model for neurons. Buffering of calcium by Calbindin is again included for completeness. ⇌ (in black color) represents reversible reactions and ⇌ (in red color) represents flow of calcium in and out of cell (and ER) by external input and pumps (SERCA and plasma membrane pumps) respectively, + sign represents positive influence on the reaction, dotted arrow represents influence of a given molecule/chemical on the reaction. $C_2$, $O_1$, $C_1$ and $O_2$ are different states for RyR receptor's calcium channels. Figure courtesy of Patrick Shoemaker.*

The figure above shows the complete trans-membrane calcium dynamics model for neurons in our model, in quasi-kinetic form. Again we include calcium buffering by Calbindin. The positive feedback loop for calcium entry into the cytosol can be described as follows: Neural input in the form of calcium influx (e.g., through NMDAR's). This influx of calcium opens RyR channels. RyR channels have calcium dependent kinetics like InP3 channels described in astrocyte model, leading to influx of more calcium from ER stores, which in response opens more RyR channels. The positive-feedback loop is limited/ terminated by nonlinear calcium pumps (SERCA and plasma membrane) and other sequestration mechanisms that remove calcium from the cytosol.

*10.3.2. Model for Ryanodine receptor (RyRs):*

The calcium flux density through ryanodine receptor channels in the ER membrane is given by an expression of the form:

$$j_R = r_{Ca} * Open_{RyR} * (C_e - C_s) \qquad 22$$

where, $r_{Ca}$ is the calcium influx density for open RyR channels, $C_e$ is the calcium concentration in endoplasmic reticulum, and $C_s$ is cytosolic calcium.

The $Open_{RyR}$ is the open probability for open RyR channels and is modeled according to [16]. It can be calculated as the sum of the two open states, $O_1$ and $O_2$ in the system of ordinary differential equations (given below), emerging from a four-state Markov model with kinetic constants $k_a^-, k_a^+, k_b^+, k_b^-, k_c^+, k_c^-$.

$$O_1 = 1 - C_1 - O_2 - C_2$$

$$\frac{dC_1}{dt} = k_a^- * O_1 - k_a^+ * C_c^4 * C_1$$

$$\frac{dO_2}{dt} = k_b^+ * C_c^3 * O_1 - k_b^- * O_2$$

$$\frac{dC_2}{dt} = k_c^+ * O_1 - k_c^- * C_2$$

*10.3.3. Model for Pumps:*

In following section we describe SERCA and Plasma membrane pumps, along with their equations.

*10.3.3.1. SERCA Pumps:*

The model for SERCA pumps in neurons is taken from [16] and is slightly modified from the model used for astrocytes. It remains essentially a 2nd order Hill equation, but with the ER calcium concentration appearing in the denominator of the expression:

$$j_{serca} = k_p^2 * \left( \frac{C_s^2}{(k_{pc} + C_s) * C_e} \right) \quad 23$$

where $k_p^2$ and $k_{pc}$ are calcium 2nd-order pump constants, $C_s$ is the cytosolic calcium concentration, $C_e$ is the local ER calcium concentration, and $j_{serca}$ is calcium efflux due to SERCA pumps. In accordance with the [16], ER calcium levels are *not* assumed to remain fixed, but are allowed to vary locally as calcium flows into the cytosol from the ER and vice-versa. Also, ER calcium concentration is treated as another state in the numerical model.

*10.3.3.2. Plasma Membrane Pumps:*

The mode for Plasma membrane pumps in neurons is taken from [16] and is expressed as first order Hill's equation:

$$j_{plasma} = k_p^1 * \left( \frac{C_s}{(k_{pc}^1 + C_s)} \right) \quad 24$$

where $k_p^1$ and $k_{pc}^1$ are calcium 1st-order pump constants, $C_s$ is cytosolic calcium and $j_{plasma}$ is calcium efflux due to plasma membrane pumps.

*10.3.4. Model for Ca Buffering:*

Model for Calcium buffering is identical to what was introduced in astrocytes section 7.2.5 and we have used the same equations as mentioned there. Refer Table 2 for parameter values.

*10.3.5. Model for Gap junction:*

Model for Gap junctions is identical to what was introduced in astrocytes section 7.2.6 and we have used the same equations as mentioned there. Refer Table 2 for parameter values.

*10.3.6. Model for leakage:*

Model for leakage is identical to that introduced in astrocytes section 7.2.7 and we have used the same equations as mentioned there. Refer Table 2 for parameter values.

| Parameter / Constants | Value | Units | Definition |
|---|---|---|---|
| DCa | 240 | $\mu m^2.s^{-1}$ | Ca diffusion coefficient in astrocytes |
| DInP3 | 300 | $\mu m^2.s^{-1}$ | InP3 diffusion coefficient in astrocytes |
| rCa | 600 | $\mu m^{-2}$ | Calcium influx rate constant for open RyR channels |
| kp1 | 75 | $\mu m.s^{-1}$ | Calcium 1st-order pump constants |
| kpc1 | 1.8 | $\mu m$ | Calcium 1st-order pump constants |
| kp2 | 4400 | $\mu m.s^{-1}$ | Calcium 2nd-order pump constants |
| kp2c | 0.10 | $\mu m$ | Calcium 2nd-order pump constants |
| K1k | 1.5 | $\mu m.s^{-1}$ | Calcium leakage rate |
| kcbf | 0.7 | $\mu m.s^{-1}$ | Rates for calcium buffering |
| kcbb | 10 | $s^{-1}$ | Rates for calcium buffering |
| CalB0 | 40 | $\mu m$ | Available Calbindin concentration |
| kAneg | 28.8 | $s^{-1}$ | RyR receptor state rates |
| kApos | 1500 | $\mu m^{-4}.s^{-1}$ | RyR receptor state rates |
| kBneg | 385.9 | $s^{-1}$ | RyR receptor state rates |
| kBpos | 1500 | $\mu m^{-3}.s^{-1}$ | RyR receptor state rates |
| kCpos | 1.75 | $s^{-1}$ | RyR receptor state rates |
| kCneg | 0.1 | $s^{-1}$ | RyR receptor state rates |
| VolR | 50 | - | Volume Ratio, Cytosol to ER |
| | | | |

*Table 2: List of Neuron Model parameter and their baseline values, along with units.*

# 11. MORPHOLOGICAL STRUCTURE OF CELLS

In our research, we are modelling astrocytes and neurons, but for simplicity we have built a morphological model of a generic "cell" that can represent both neurons and astrocytes. Astrocytes are star-shaped cells that have radiating cellular processes that we will refer to as 'dendrites' for simplicity (even though dendrite is usually used to refer to a form of neural process). Every cell in our model has a stereotyped morphology and is made of 3 morphological subunits: a cell body (or more precisely, the region at which the dendrites meet), straight dendrites and branched dendrite. And, these subunits are composed of compartments, which can be regarded as defining discrete finite elements or a *grid* for our signal propagation model. The dendrite model is one-dimensional (analogous to cable models for electrical behavior) and thus this grid is one-dimensional. The cell body is itself a single compartment. Straight dendrites are made of 10 compartments each and every cell has 8 straight dendrites. Branched dendrites are made of 3 segments and these segments are made of 5 compartments each, and we have 4 branched dendrites in our model. To characterize the state of the compartments, a storage structure is been defined in the simulation code that maintains the value of required states (which include for example $[Ca^{2+}]$, [DAG], $[InP_3]$, and other states for the local receptor populations).

Below in Figure 7 is a diagram of our model cell, having one cell body, eight straight dendrites, and four branched dendrites with a total of 12 dendrites.

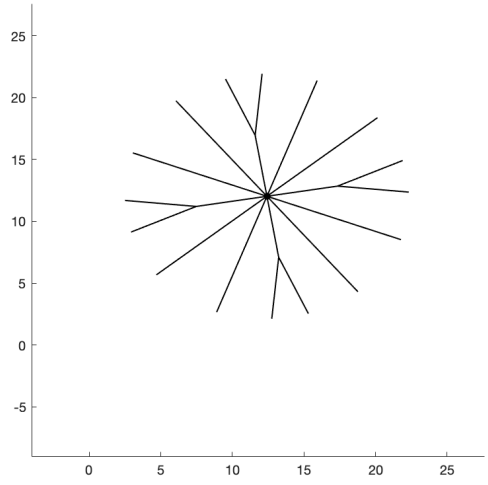


*Figure 7: Single cell in our model.*

Figure 8 is an image of 4 cells interconnected together through some randomly-placed interconnections (red dots), corresponding to gap junctions. In a typical network, we may have hundreds of such cells interconnected together.

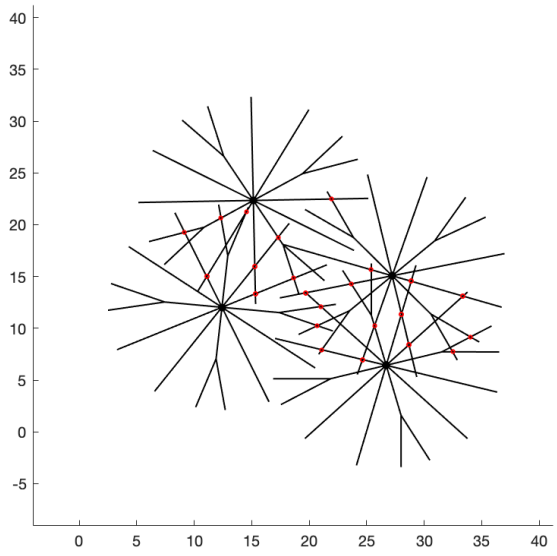


*Figure 8: Two interconnected cell in our model. Red dots represent gap junction interconnections.*

## 12. NUMERICAL SIMULATION

We simulate the propagation of calcium waves in network of cells arranged in a two-dimensional network and in individual dendrites as well. Network modeling only looks at networks of the astrocytes, and not networks of neurons. Our work on neurons is limited to dendritic propagation only. We aren't clear on how calcium waves would be transmitted from neuron to neuron, although it might be either by synapses or gap junctions, and furthermore the neural model is complicated by the fact that calcium entry typically causes depolarization as well.

These network simulations are carried out using Matlab scripts. One script generates network of these cells with a stereotypical architecture, but with randomness introduced in their placement and orientation. Cells are placed on a hexagonal grid for symmetry, but random offsets in the x and y directions are added to the cell positions, and they are rotated randomly at placement. Below in Figure 9 you can see a skeletonized diagram of a network of 16 astrocytes interconnected to each other.

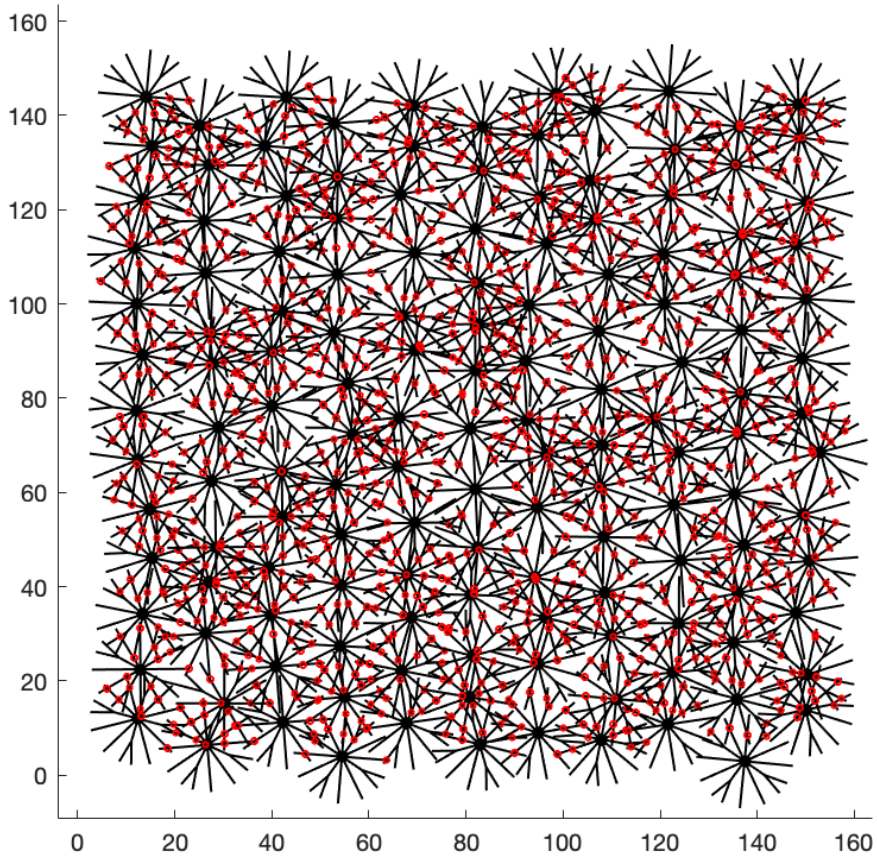


*Figure 9: Network of 143 astrocytes interconnected together. Red dots represent gap junction interconnections.*

### *12.1. Mathematical Formulation:*

Our model (dendrites and cell body) is discretized into compartments and calcium is transported laterally between compartments by diffusion, and trans-membrane calcium flux (and buffering) is calculated locally at each compartment.

We can divide the trans-membrane components of our model into two -- 1) Source component: it increases the (current) calcium concentration by providing positive feedback or by directly adding more calcium ions (e.g. receptor channels (InP3 and RyR), leakage) and 2) Sink component: it decreases the (current) calcium concentration by directly pumping out or removing calcium ion (e.g. pumps, buffering of calcium is also treated as sink since it removes free calcium from the cytosol). So, after incorporating these two components, our model equation can be written as:

$$\frac{\partial}{\partial t}[Ca^{2+}] = D_{Ca}\frac{\partial}{\partial x^2}[Ca^{2+}] + j_{s_{rc}} - j_{s_{nk}} \qquad 25$$

where, $j_{s_{rc}}$ represent source terms and $j_{s_{nk}}$ represent sink terms.

In order to solve this equation numerically, we are using MOLE (*Mimetic Operators Library Enhanced*) library (discussed in 12.3) to do spatial integration and for temporal integration we are doing simple quadrature, i.e. multiplying the equation 25 by a finite time increment $\Delta t$ and summing over time.

*12.2. Numerical Solution:*

We have solved our model numerically using Mimetic Discretization Methods [17]. After discretizing our domain, the model can be written in matrix-vector format given by following equation;

$$U^{n+1} = L * U^n + (S_{rc} + S_{nk}) \qquad 26$$

where, $L$ is our mimetic Laplacian operator (matrix) and $S_{rc}$ and $S_{nk}$ are vectors that represent flux from source and sink components in our model.

We construct 1D mimetic Laplacian operator $L$ using MOLE library. This operator returns a sparse matrix of size *(m+2)* by *(m+1)* is called using a command in Matlab, "*lap(k, m, dx)",* as shown below.

$$L = lap\,(k, m, dx)$$

where, k is operator's order of accuracy, m is the number of cells required to attain the desired accuracy, dx is the step size along x-axis.

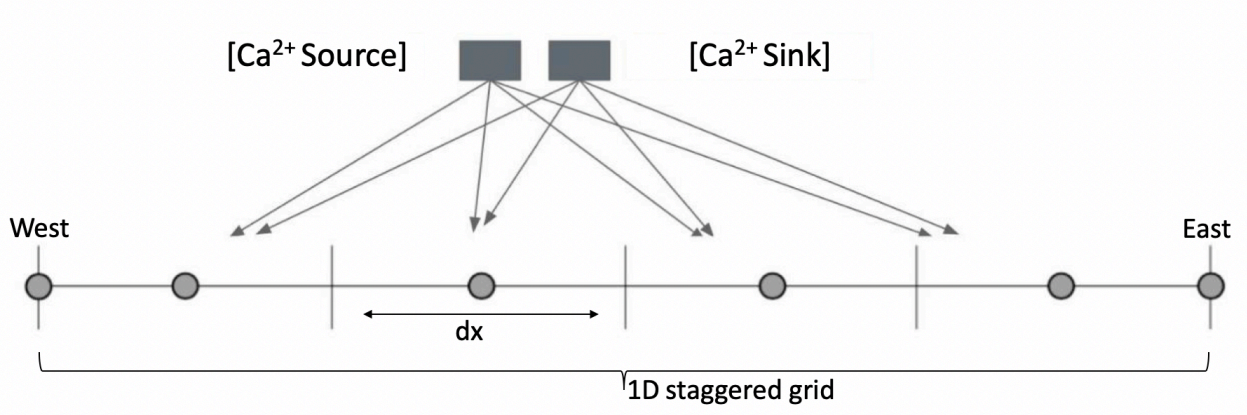


*Figure 10: 1D staggered grid with Ca source and sink acting on every grid point.*

Generating an array of 1D staggered grid points and storing them in "*grid*" is done in Matlab as shown below,

$$grid = [\,west \quad west + dx/2 : dx : east - dx/2 \quad east\,]$$

where, *west* and *east* are two ends of our *grid* and *dx* is the step size on x-axis. We have calcium source and sink terms acting on every grid point and it can be visualized as shown in Figure 10.

*12.3. Boundary Conditions:*

As per assumptions in our model, dendrites are sealed at one end (flux = 0), and the flux out at the other end must be set to match the flux into the cell body. And, similarly fluxes out of cell body on the other end must match the sum of fluxes from the dendrites. This requires a Robin boundary condition, which is a weighted combination of Dirichlet boundary conditions and Neumann boundary conditions. In MOLE library, this can be imposed using following statement:

$$BC = robinBC(k, m, dx, a, b)$$

where, k is operators order of accuracy, m is the minimum number of cells required to attain the desired accuracy, dx is the step size along x-axis, a = 0 and b = 1 are coefficients in robin boundary conditions.

*12.4. MOLE Library:*

MOLE (Mimetic Operators Library Enhanced) is a high quality (C++ and Matlab) library that implements high-order mimetic operators to solve partial difference equations. It provides discrete analogs of the most vector calculus operators: *Gradient*, *Divergence*, *Laplacian* and *Curl.* These operators (matrices) act on staggered grids (uniform and non-uniform) and they satisfy local and global conservation laws. The mathematics of MOLE is based on the work of [17].

# 13. EXPERIMENTATION:

In this section we will discuss how experiments were designed and carried out. We have done hundreds of experiments if not more to understand:

1. The dynamics of Ca waves in a single and a network of astrocytes/ neurons.
2. What are the parameters that effect the wave speed, wave amplitude, regenerative mechanics, damping behavior.

*13.1. Design of experiments:*

We can break down the experiments into following categories:

A.) Different types of test beds:
   a) Single dendrite
   b) Two dendrites connected through cell body
   c) Two cells connected end-to-end through two dendrites
   d) Network of complete cells interconnected to each other randomly

B.) Varying different parameters:
   a) Changing one parameter at a time
   b) Changing multiple parameters simultaneously
   c) Changing two parameters together while keeping others at their baseline value.

| Parameter | Definition |
|---|---|
| kd1f | Ca-dependent production of InP3 |
| kaa | Ca-influx rate for open ARC channels |
| fCa | Fraction to reduce DCa due to intracellular crowding |
| fInP3 | Fraction to reduce DInP3 due to intracellular crowding |
| kCa | Calcium influx rate constants for open InP3 channels |
| rCa | Calcium influx rate constants for open RyR channels |
| kGI | Rate of InP3 production induced by glutamatergic input |
| kcbf | Rates for Ca buffering |
| kcbb | Rates for Ca buffering |
| ki2 | Inhibition of InP3 production by PKC |

*Table 3: Model parameters and rate constants that are varied in experiments for Astrocyte model. All these parameters are also shown in Table 1, we are re-iterating these for better clarity.*

*13.2. Initiation of Waves:*

We initiate waves (in cells or a network) through simulated stimuli. We can think of stimulus as a input received by our network that triggers an influx of calcium and leads to propagation of calcium waves. This input may be received at a fixed location ( in a single compartment) or in a region of a network (multiple cells/ dendrites); it can either be a stationary or a moving input that excites a succession of locations in the network.

We model stimuli in astrocytes with temporal pulses of the G-protein ($G_\alpha$) which result in generation of InP3 in a region defined in the simulation code. The G-protein concentration during such pulses is represented by $G_{in}$ which appears in equation 11. If stimulus is applied to a point (compartment) in our model, G-protein pulse is activated for $t_{stim}$ seconds and when it is applied to an area, there is a finite $G_{in}$ value for all compartments within the radius of influence ($r_{max}$) of the stimulus. Furthermore, the area of stimulus influence can move ($Vel_{stim}$) in time, with pulses applied to successive compartments when they are within the area. All the parameters that define stimulus are given in Table 4, as shown below.

| Parameter | Values | Units | Definition |
|---|---|---|---|
| kGI | 40 | $\mu m.s^{-1}$ | Rate of InP3 production induced by glutamatergic input |
| $r_{max}$ | 1 | μm | Radius of influence |
| $Vel_{stim}$ | YE/ $t_{end}$ | $\mu m.s^{-2}$ | Stimulus speed |
| $t_{stim}$ | 1/8 * $t_{end}$ | s | Terminate stimulus after $t_{stim}$ seconds |
| $X_{stim}$ | - | μm | x-location of stimulus |
| $Y_{stim}$ | - | μm | y-location of stimulus |

*Table 4: Parameters related to stimulus. Changing these parameters we can change the strength or region of influence of stimulus in our network.*

# 14. RESULTS:

In a series of experiments varying different parameters on different test beds, we examined how each model parameter impacts propagating of Ca waves in dendrites of neurons and astrocytes.

The factors or characteristics that we are interested in examining are as follows:

1. Regenerative: How does model parameter impacts the ability of waves to regenerate itself, so that it can propagate for long distance, before it dies out (if it does)?
2. Damping Wave: Does wave gets damped, i.e., decrease in amplitude as it propagates, because of some parameter value?
3. Wave speed: Does wave speed increase or decrease with change in parameter values?
4. Wave amplitude: Does amplitude of wave increase, decrease or remains unchanged with change in parameter value?
5. Region of influence: Does given parameter have local or global effect in our model? A parameter having local influence will affect wave properties locally, whereas, a parameter having global influence will affect the wave properties throughout the model.

In order to better understand the impacts of different parameters on Ca waves, we have divided our analysis into two parts:

## *14.1. Qualitative Analysis:*

Here we analyze qualitatively how does wave behaves on different test beds with change in parameter values. And, these qualitive results are expressed as:

### *14.1.1. Qualitative Analysis Chart:*

We have created a chart of model parameters summarizing effects of parameters on different wave characteristics or factors as mention in previous section.

| Parameters | Regeneration | Damping | Wave Speed | Wave Amplitude | Effect |
|---|---|---|---|---|---|
| kd1f | Strong Positive | Strong Negative | Strong Positive | Strong Positive | Global |
| kaa | Positive Indirect | NO EFFECT | Positive | NO EFFECT | Global |
| fCa | Strong Negative | Strong Positive | Strong Negative | Strong Negative | Global |
| fInP3 | Strong Negative | Strong Positive | Strong Positive | Strong Positive | Global |
| kCa | Positive | Strong Negative | Strong Positive | Strong Positive | Global |
| kGI | NO EFFECT | NO EFFECT | Positive | Small Positive | Local |
| rInP3 | Small Positive | NO EFFECT | Small Positive | NO EFFECT | Local |
| kcbf | Strong Negative | Strong Positive | Strong Negative | Strong Negative | Global |
| kcbb | Strong Positive | Strong Negative | Positive | Strong Positive | Global |
| Ki2 | Strong Negative | Strong Positive | Strong Negative | Strong Negative | Global |

*Table 5: Chart for model parameters and its effects on the Ca wave dynamics. Strong Positive means that the quantity (like speed) becomes larger or the phenomenon becomes more pronounced when the parameter increase. Strong Negative means that the quantity (like speed) becomes smaller or the phenomenon diminishes as the parameter increase. NO EFFECT means that change in parameter value*

*have no effect on the wave. Small positive and Small negative means that increase in parameter value will have small (less-strong) impact on the wave. Local and Global means whether the change in parameter value locally will impact locally or globally.*

*14.1.2. Different Regimes for Calcium waves:*

Our experiments demonstrate that there are regenerative, damping and abortive regimes for calcium waves, depending on the physiological parameters. In regenerative regime, calcium waves can travel through the entire network of cells (along dendritic distances) by regenerating itself. In damping regime, calcium waves gets damped as it propagates and could die before it reaches till the end of network. We further observe that abortive regime exist, where our model is not able to generate waves that could propagate even a few micrometers.

Table given below gives the different ranges of parameter values that give different wave behavior. We selected *reference values* for these parameters, which appear to be physiologically reasonable and in combination give traveling wave behavior We call these *reference value* as the *base line value* for that parameter. By default all parameters are set to their baseline values.

| Parameters | Regenerative waves | Damping waves | Abortive regimes | Baseline value |
|---|---|---|---|---|
| kd1f | >= 5 | 4 < kd1f < 3 | < 4 | 5 |
| kaa | > 4 | 4 < kaa < 2 | < 2 | 6 |
| fCa | < = 0.3 | 0.3 < fCa < 0.5 | > 0.5 | 0.3 |
| fInP3 | > 0.7 | 0.7 < finp3 > 0.5 | < 0.5 | 0.7 |
| kCa | > 500 | 500 < kCa< 400 | < 400 | 600 |
| kcbf | < 1 | 1 < kcbf < 4 | > 4 | 0.7 |
| kcbb | > 5 | 5 < kcbb < 3 | < 3 | 10 |
| ki2 | < 1 | 1 < ki2 < 5 | > 5 | 0.0943 |

*Table 6: Table for range of parameter values for different wave behavior. Every parameter is varied separately while keeping other parameters at their baseline value. All experiments were performed on a test bed of two cells with two dendrites each.*

*14.1.3. Regeneration Mechanism:*

We have observed (as shown in Table 5) all the parameters (except kGI) either increase or decrease the strength of regenerative mechanism, while kGI has no effect.

*14.1.4. Damping Behavior:*

Among all parameters, kaa, kGI and rInP3 have no effect on the damping behavior of calcium waves. And, fCa, fInP3, kcbf and ki2 increases the damping behavior as we increases their values, whereas kd1f, kCa, kcbb decreases the damping behavior.

*14.1.5. Wave Speed:*

Parameters that increases wave speed are: kd1f, kGI, kaa, kCa and kcbb, whereas those decrease it are ki2, kcbf, and fca.

*14.1.6. Wave Amplitude:*

We can see from the Table 5 that only two parameters, kaa and rInP3 have no effect on amplitude of calcium waves and all other parameters either increase or decrease wave amplitude.

*14.1.7. Region of Influence:*

Region of Influence is a qualitative measure to analyze, whether the change in value of given parameter will have impact on waves throughout the model or just locally. We have found that except kGI and rInP3, all parameters have global effect on any change in value, whereas kGI and rInP3 have localized effect. Any change in kGI and rInP3 in a specific region will not affect the dynamics of Ca waves in other regions of model.

This make sense physically as well, because these two parameters (kGI and rInP3) presence is physically limited to the certain region of the model. For example, kGI which defines the strength of stimulus/ input to our model, is active only for $t_{stim}$ sec and that too only in one region (or direction), after which it has zero effect on our model. Similarly, rInP3 which defines the strength of exchange of InP3 between two cells/ dendrites through gap junctions is limited physically as gap junctions are only presents at the interconnections between cells/ dendrites. So, exchange of calcium happens only in certain regions locally.

*14.2. Quantitative Analysis of calcium waves in dendrites:*

In this section, we show quantitative results for all the experiments, analyzing wave speed and amplitude.

*14.2.1. Astrocytes Model:*

In the below given Table 7 and Table 8, we show how wave speed and amplitude change with change in parameter values. The values in first column corresponds to a parameter (for e.g. kd1f) and the values in the next column are speed of waves because of the parameter in first column. Similarly, values in third column corresponds to parameter kaa and values in fourth column are wave speed because of kaa. Wave speed is represented by V.

| kd1f | *V* | kaa | *V* | fCa | *V* | fInP3 | *V* | kCa | *V* | kGI | *V* | Ki2 | *V* | kcbf | V | kcbb | V |
|---|---|---|---|---|---|---|---|---|---|---|---|---|---|---|---|---|---|
| 8 | 37.7 | 9 | 33.8 | 1 | 29.8 | 1 | 38.4 | 1500 | 105.2 | 120 | 38.4 | 5 | 20.0 | 5 | 0 | 14 | 34.4 |
| 7 | 35.7 | 8 | 33.3 | 0.8 | 30.7 | 0.8 | 34.4 | 1200 | 95.2 | 100 | 37.7 | 3 | 24.6 | 3 | 15.8 | 10 | 33.3 |
| 6 | 33.3 | 6 | 33.3 | 0.6 | 31.7 | 0.7 | 33.3 | 900 | 83.3 | 80 | 37.0 | 1 | 29.8 | 1 | 2 | 6 | 30.7 |
| 4 | 21.2 | 4 | 32.2 | 0.3 | 33.3 | 0.5 | 28.1 | 600 | 33.3 | 45 | 33.3 | 0.5 | 32.2 | 0.7 | 33.3 | 3 | 27.0 |
| 2 | 0 | 2 | 31.2 | 0.2 | 32.7 | 0.3 | 19.2 | 400 | - | 20 | 22.4 | .09 | 33.3 | 0.3 | 38.4 | 1 | 19.4 |
| 0 | - | 0 | - | 0 | 29.8 | 0 | - | 0 | - | 10 | - | 0 | 0 | 0 | - | 0 | 19.4 |
| | | | | | | | | | | | | | | | | | |

*Table 7: Table for Wave velocity (V) with change in parameter value. All experiments are done on a 100 compartment-long single dendrite, where every parameter was varied individually while others were kept constant at their baseline values. Values in red color in e every column indicate the baseline value for that parameter. "-" represents no wave for that set of parameter values. Units for V is* $\mu m.s^{-1}$.

Table 8 shows change in wave amplitude as parameters are varied; results are arranged as per previous table, first column corresponds to a parameter and subsequent column shows change in wave amplitude because of values in first column . Wave amplitude is represented by A with units in uM/s.

| kd1f | *A* | kaa | *A* | fCa | *A* | fInP3 | *A* | kCa | *A* | kGI | *A* | Ki2 | *A* | kcbf | A | kcbb | A |
|---|---|---|---|---|---|---|---|---|---|---|---|---|---|---|---|---|---|
| 8 | 4 | 10 | 2.6 | 1 | 1 | 1 | 3.1 | 1500 | 15.4 | 120 | 3 | 5 | 0.9 | 5 | 0 | 14 | 2.9 |
| 7 | 3.2 | 8 | 2.6 | 0.8 | 1 | 0.8 | 2.6 | 1200 | 12.7 | 100 | 2.9 | 3 | 1.2 | 3 | 1 | 10 | 2.3 |
| 6 | 2.3 | 6 | 2.3 | 0.6 | 1.4 | 0.7 | 2.3 | 900 | 9.7 | 80 | 2.8 | 1 | 1.8 | 1 | 2 | 6 | 1.8 |
| 4 | 1 | 4 | 2.3 | 0.3 | 2.3 | 0.5 | 1.8 | 600 | 6.1 | 45 | 2.3 | 0.5 | 2 | 0.7 | 2.3 | 3 | 1.4 |
| 2 | 0 | 2 | 2.2 | 0.2 | 3.7 | 0.3 | 1.1 | 400 | 3.9 | 20 | 1.4 | 0.09 | 2.3 | 0.3 | 3.2 | 1 | 0.8 |
| 0 | - | 0 | - | 0 | 5.8 | 0 | - | 0 | - | 10 | 0 | - | 2.5 | 0 | - | 0 | 0.7 |
| | | | | | | | | | | | | | | | | | |

*Table 8: Table for Wave amplitude (A) with change in parameter value . All experiments are done on a 100 compartment-long single dendrite, where every parameter was varied once (while others were kept constant at their baseline value). Values in red color in every column are the baseline value for that parameter. "-" represents no wave for those set of parameter value. Units for A is μm.*

### *14.2.2 Neuron Model:*

Below given two tables shows, how wave speed and amplitude change with change in different parameter values for a neuron model.

| fCa | *V* | rCa | *V* | kcbf | V | kcbb | V |
|---|---|---|---|---|---|---|---|
| 1 | 416.66 | 100 | $1.2e^{+03}$ | 10 | - | 100 | 454.54 |
| 0.8 | 384.61 | 50 | 1000 | 5 | 156.25 | 50 | 454.54 |
| 0.6 | 333.33 | 20 | 714.28 | 1 | 384.61 | 35 | 416.66 |
| 0.4 | 263.15 | 10 | 555.55 | 0.7 | 416.66 | 20 | 416.66 |
| 0.2 | 178.57 | 5 | 416.66 | 0.3 | 454.54 | 10 | 416.66 |
| 0 | - | 0 | - | 0 | 500 | 0 | 416.66 |
| | | | | | | | |

*Table 9: Table for Wave speed (V) with change in parameter value . All experiments are done on a single dendrite, where every parameter was varied once (while others were kept constant at their baseline value). Values in red color in every column are the baseline value for that parameter. "-" represents no wave for those set of parameter value. Units for V is μm.$s^{-1}$.*

In general, wave speed (*V*) decrease as you decrease fCa and rCa (and vice-versa). As far as buffering is concerned:

1. kcbf: As we increase kcbf, wave speed decreases.
2. kcbb: More or less, change in kcbb doesn't change wave speed. But there seem to be a point at which there is a slight increases in velocity.

| fCa | *A* | rCa | *A* | kcbf | A | kcbb | A |
|---|---|---|---|---|---|---|---|
| 1 | 3 | 100 | 5.2 | 10 | - | 100 | 3.2 |
| 0.8 | 3 | 50 | 4.8 | 5 | 1 | 50 | 3.2 |
| 0.6 | 3 | 20 | 4.2 | 1 | 2.8 | 35 | 3 |
| 0.4 | 3 | 10 | 3.8 | 0.7 | 3 | 20 | 3 |
| 0.2 | 3 | 5 | 3 | 0.3 | 3.5 | 10 | 3 |
| 0 | - | 0 | - | 0 | 3.9 | 0 | 3 |
| | | | | | | | |

*Table 10: Table for Wave amplitude (A) with change in parameter value . All experiments are done on a single dendrite, where every parameter was varied once (while others were kept constant at their baseline value). Values in red color in every column are the baseline value for that parameter. "-" represents no wave for those set of parameter value. Units for A is μm.*

In general, wave amplitude (*A*) decrease as you decrease rCa and vice-versa. fCa doesn't have any impact on amplitude of waves. As far as buffering is concerned:

1. kcbf: As we increase kcbf, wave amplitude decreases and vice-versa.
2. kcbb: No effect on wave velocity.

*14.2.3. Combination of parameters:*

In this section, we varied different combinations of parameters together to study how they affected wave speed in a single dendrite. We varied all parameters varied in pairs of two while others were kept at their baseline value as mentioned in Table 7.

| Pair 1: fCa and fInP3 | | | |
|---|---|---|---|
| fCa | fInP3 | Wave Speed | Wave Amp. |
| 0.5 | 0.5 | 15.74 | 0.6 |
| 0.5 | 1 | 36.36 | 1.8 |
| 1 | 0.5 | - | - |
| 1 | 1 | 31.74 | 0.8 |

| Pair 2: fCa and kCa | | | |
|---|---|---|---|
| fCa | kCa | Wave Speed | Wave Amp. |
| 0.5 | 300 | - | - |
| 0.5 | 600 | 25.97 | 1 |
| 1 | 300 | - | - |
| 1 | 600 | 17.85 | 0.5 |

| Pair 3: fCa and kaa | | | |
|---|---|---|---|
| fCa | kaa | Wave Speed | Wave Amp. |
| 0.5 | 3 | 24.09 | 1 |
| 0.5 | 8 | 27.77 | 1.2 |
| 1 | 3 | - | - |
| 1 | 8 | 21.50 | 0.5 |

| Pair 4: fCa and kd1f | | | |
|---|---|---|---|
| fCa | kd1f | Wave Speed | Wave Amp. |
| 0.5 | 3 | - | - |
| 0.5 | 6 | 33.33 | 1.7 |
| 1 | 3 | - | - |
| 1 | 6 | 29.41 | 1 |

| Pair 5: fInP3 and kCa | | | |
|---|---|---|---|
| fInP3 | kCa | Wave Speed | Wave Amp. |
| 0.5 | 300 | - | - |
| 0.5 | 600 | 21.27 | 1.2 |
| 1 | 300 | - | - |
| 1 | 600 | 38.46 | 2.4 |

| Pair 6: fInP3 and kaa | | | |
|---|---|---|---|
| fInP3 | kaa | Wave Speed | Wave Amp. |
| 0.5 | 3 | 20.00 | 1 |
| 0.5 | 8 | 22.72 | 1.2 |
| 1 | 3 | 37.73 | 2.4 |
| 1 | 8 | 39.21 | 2.6 |
| Pair 7: fInP3 and kd1f | | | |
| fInP3 | kd1f | Wave Speed | Wave Amp. |
| 0.5 | 3 | - | - |
| 0.5 | 6 | 27.39 | 1.8 |
| 1 | 3 | - | 0.8 |
| 1 | 6 | 42.55 | 3.8 |
| Pair 8: kCa and kaa | | | |
| kCa | kaa | Wave Speed | Wave Amp. |
| 300 | 3 | - | - |
| 300 | 6 | - | - |
| 600 | 3 | 33.89 | 2.36 |
| 600 | 6 | 34.48 | 2.5 |
| Pair 9: kCa and kd1f | | | |
| kCa | kd1f | Wave Speed | Wave Amp. |
| 300 | 3 | - | - |
| 300 | 6 | - | - |
| 600 | 3 | - | - |
| 600 | 6 | 34.48 | 2.4 |
| Pair 10: kaa and kd1f | | | |
| kaa | kd1f | Wave Speed | Wave Amp. |
| 3 | 3 | - | - |
| 3 | 6 | 33.89 | 2.4 |
| 8 | 3 | - | - |
| 8 | 6 | 35.08 | 2.6 |

### *14.3. Calcium Wave behavior in network of Astrocytes:*

In following section, we show theoretical and empirical results for wavefront speed in a densely inter-connected network of astrocytes.

#### *14.3.1. Wavefront in a network:*

The (random) arrangement of cells (astrocytes and neurons) in our model creates a complicated network/ structure as shown in Figure 9, which makes it difficult for a wave to propagate with similar dynamics as it does in 1-dimensional dendrite. Any such propagation will have rich spatial structure and significantly reduced wave speed. In this section, we review how wavefront (speed is reduced as) wave propagates through a network of astrocytes.

Defining a wavefront is a difficult task as it involves, considering delays because of cell body, gap junctions and mis-alignment between dendrites and the overall direction of propagation. To make computation simpler we first define an approximation that is considering only 1) waves as they are passing through dendrites in a network – i.e., the effects of cell bodies and gap junctions are not being considered here, and 2) the plane wave approximation, which is an approximation to a wavefront with a large radius. It is therefore a crude estimate that is taking into account only the fact that dendrites can mis-align with the overall wavefront direction. The wave will be slowed down further by cell bodies and gap junctions.

### *14.3.2. Theoretical computation of wavefront speed:*

In following section we show theoretical computation for wavefront speed in a network, where a plane wave approximation is made. This approximation accounts for propagation in the dendrites only and neglects any delays because of gap junctions and cell body.

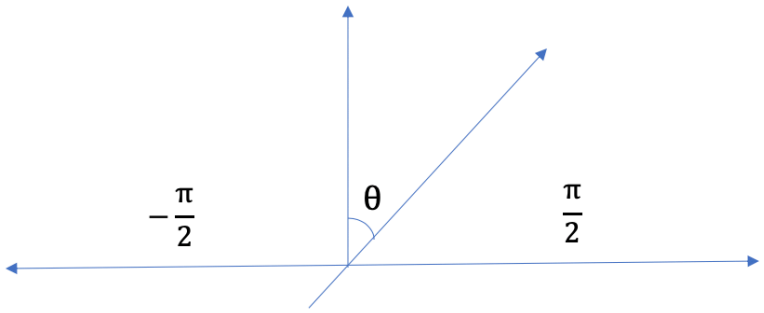


*Figure 11: Plane wave approximation. $\theta$ is the angle between direction of wave front and perpendicular to plane wave. Dendrites are uniformly distributed with respect to $\theta$ and can be anywhere from -90$^o$ to 90$^o$.*

Because of the random orientations, dendrites in our models are distributed uniformly according to the angle they make with respect to the wavefront. We can represent this as a probability distribution $f(\theta)$, with our angular domain going from - $\frac{\pi}{2}$ $to$ $\frac{\pi}{2}$.

$$\int_{-\frac{\pi}{2}}^{\frac{\pi}{2}} f(\theta)d\theta = 1$$

Since, $f(\theta)$ follows uniform distribution, probability density can be represented as constant $c$.

$$\int_{-\frac{\pi}{2}}^{\frac{\pi}{2}} c * d\theta = 1$$

$$c * \pi = 1$$

$$c = \frac{1}{\pi}$$

We integrate velocity component $v_{den}\cos(\theta)$ against uniform distribution.

$$v_{avg} = c * \int_{-\pi/2}^{-\pi/2} v_{den}\cos(\theta)\, d\theta$$

$$v_{avg} = c * v_{den} * \int_{-\pi/2}^{-\pi/2} \cos(\theta)\, d\theta$$

$$v_{avg} = c * v_{den} * \left[sin\left(\frac{\pi}{2}\right) - sin\left(-\frac{\pi}{2}\right)\right]$$

$$v_{avg} = c * v_{den} * 2$$

$$v_{avg} = \frac{2 * v_{den}}{\pi}$$

So, this gives us an average dendritic wave speed in a network, where $v_{den}$ is wave speed in a single dendrite. With this estimate, we can say average wave front speed in a network should be approximately equal to 2/3 of the wave speed in a dendrite, ignoring transmission through cell bodies and gap junctions.

Now using wave speed values in a dendrite from Table 8 and Table 10, we can estimate what would be average wavefront speed in any astrocyte/ neuron network respectively. For astrocytes, wave speed in a single dendrite with baseline parameter values, represented as $v_{den}$ is 33.33 μm.s$^{-1}$. So, wavefront speed can be computed as:

$$v_{astrocyte} = \frac{2 * 33.33}{\pi} \cong 21\frac{\mu m}{s}$$

For neurons, wave speed in a single dendrite with baseline parameter values, represented as $v_{den}$ is 416.16 um/s$^2$. So, wavefront speed can be computed as:

$$v_{neuron} = \frac{2 * 416.66}{\pi} \cong 265\frac{\mu m}{s}$$

This gives us a theoretical estimate that is an upper bound for wavefront speed in astrocyte ($v_{astrocyte}$) and neural ($v_{neuron}$) networks.

*14.3.3. Observed Wavefront speed:*

In order to compute wavefront speed in a network, we define wavefront in terms of (single) farthest compartment in each cell that experience a calcium wave peak. As wave gets initiated in a network, it propagate through the cells and spreads across the network, we look at the compartment in each cell that is activated by wave and is farthest from the origin. Origin in a network is the compartment/ point where these waves are started. We define cell body of the center most cell in

our network (for e.g. 13 by 15 network) as the origin in all our experiments. Then, distance of that compartment from the origin is divided by time taken for wave peak to occur in that compartment, this gives us the speed. This speed is than averaged for all cells in our network, which gives us wavefront speed.

Below are the empirical results from our wave front speed measurement experiments. All the parameters were set to their baseline values as mentioned in Table 6. We can see our empirical results are less than our theoretical results (as shown in section 14.3.2.) and this is because of the delays caused by cell bodies and gap junction transmission.

| Network Size (m by n) | Wavefront Speed ($\mu m.s^{-1}$) |
|---|---|
| 3 by 4 | 16.66 |
| 5 by 5 | 17.34 |
| 7 by 7 | 14.94 |
| 10 by 9 | 14.78 |
| 11 by 13 | 14.67 |
| 13 by 15 | 14.12 |

*Figure 11: Table for wavefront speed measurement in different networks of cells (astrocytes). Network of size m by n, have m*n cells, arranged on a grid of m by n. All the parameters were set to their baseline values as mentioned in Table 7 above.*

# 15. CONCLUSION:

We have studied, modeled and examined calcium wave propagation primarily in astrocytes in three different ways: 1) in individual dendrites, 2) in two interconnected cells with two dendrites each and 3) in a network of up to few hundred cells.

With the parameters values reported in Table 1, we have observed propagation speed in an individual dendrite is in the range 20-40 $\mu m.s^{-1}$, however there are cases where we have observed speed of more than 100 $\mu m.s^{-1}$ (shown in Table 7). The lower end of the range is consistent with the speed of the some of the faster calcium waves observed in vertebrate astrocytes [9,10] and shows that higher speeds are attainable with appropriate parameter values. Wave amplitudes in astrocytes are in the range 1.2-12 μm. which is consistent with most physiological results in vertebrates

In an network of astrocytes, however, the net speed of a wavefront that spans many cells will be slower than dendritic speed, because of random orientation of dendrites with respect to wave propagation. Also, propagation of wave through gap junctions and cell body will adds delays. We show this both theoretically (in section 14.3.2) and empirically (in section 14.3.3). As per theoretical estimates, wavefront speed in a network with baseline parameter values is 21μm/s and as per empirical observations, wavefront speed is approx. 14 $\mu m.s^{-1}$. This difference between theoretical and empirical results is because of delays added by gap junctions and cell body.

The range of wave speed in astrocyte dendrites and networks is slow, however, we have observed that speed on a scale of ~100 $\mu m.s^{-1}$ can be achieved with higher receptor density, which is

conceivable for propagation facilitation. But this is likely that these higher receptor density are unrealistic. So, we conclude astrocytes network is unlikely be the substrate to support propagating facilitation in the primary lobula of dragonflies, but it is conceivable that such networks might serve this function in smaller subregions of the brain, such as the medial lobula. However, dendritic wave speed in neurons mediated by RyRs has been observed to have much faster dynamics. Waves in the range of 150-500 $\mu m.s^{-1}$ has been observed (refer to Table 9). Thus, our preliminary conclusion is that neuronal calcium waves may indeed be sufficient to support facilitation at the level of primary lobula.

# REFERENCES:


1. Corbet, P.S. (1999): Dragonflies: Behavior and Ecology of Odonata. Ithaca, NY: Cornell Univ Press.
2. Nordstrom, K., Barnett, P.D., and O'Carroll, D.C. (2009): Insect detection of small moving targets moving in visual clutter. PLoS Bolo. 4:e54. DOI: 10.1371/journal.pbio.0040054
3. Wiederman and O'Carroll, D.C. (2013): Selective attention in an insect visual neuron. DOI: 10.1016/j.cub.2012.11.048.
4. Marisa Brini, Tito Call, Denis Ottolini, and Ernesto Carafoli (2014): Neuronal calcium signaling: function and dysfunction
5. Michael J Berridge 1998: Neuronal Calcium Signaling. DOI: 10.1016/s0896-6273(00)80510-3
6. Dunbier, Wiederman, Shoemaker, O'Carroll (2012): Facilitation of dragonfly target-detecting neurons by slow moving features on continuous paths . DOI: 10.3389/fncir.2012.00079
7. J.E. Castillo and R.D. Grone (2003), A Matrix Analysis Approach to Higher-Order Approximations for Divergence and Gradients Satisfying a Global Conservation Law. SIAM J. Matrix Anal. & Appl., 25, 128–142.
8. Shoemaker (2018): Mechanism for Spatiotemporal Visual Feature Detection in Insects. Progress Report 2, March 31, 2018. FA9550-16-1-0153
9. Bazargani and Atwell, (2016): Astrocyte calcium signaling: the third wave. Nat Neurosci. 2016 Feb;19(2):182-9. DOI: 10.1038/nn.4201.
10. Jaffe and Creton, (1998): Patterns of free calcium in zebrafish embryos. J Cell Sci. 1998 Jun; 111 (Pt 12):1613-22.
11. Scemes E, Giaume C. (2006): Astrocyte calcium waves: What they are and What they do. DOI: 10.1002/glia.20374.
12. Wiedermen (2017): A predictive focus of gain modulation encodes target trajectories in insect vision. eLife 2017;6:e26478, DOI: 10.7554/eLife.26478
13. Shuttleworth (2009): Arachidonic acid, ARC channels, and Orai proteins: DOI: 10.1016/j.ceca.2009.02.001
14. Minchul Kang, Hans G Othmer (2009): Spatiotemporal Characteristics of Calcium Dynamics in Astrocytes. DOI: 10.1063/1.3206698
15. James Sneyd and Jean-Francois Dufour (2002): A dynamic model of the type-2 inositol triphosphate receptor. DOI: 10.1073/pnas.032281999
16. Markus Breit and Gillian Queisser (2018): What is required for Neuronal Calcium Waves? A Numerical Parameter Study. DOI: 10.1186/s13408-018-0064-x
17. Johnny Corbino and Jose E.Castillo (2020): High-order mimetic finite-difference operators satisfying the extended Gauss divergence theorem. DOI: 10.1016/j.cam.2019.06.042
18. J. Sneyd (2018): In personal communication over email in regard to Gap junctions.
19. Golovina and Blaustein, (2000): Unloading and refilling of two classes of spatially resolved endoplasmic reticulum Ca(2+) stores in astrocytes. PMID:10816603
20. Berrideg MJ, 1998: Neuronal Calcium Signaling. DOI:10.1016/s0896-6273(00)80510-3
21. TJ Shutterworth, (2009): Arachidonic acid, ARC channels, and Orai proteins. PMCID:PMC2744097
22. Reyes, Verkhratsky, and Parpura (2012): Plasmalemmal $Na^{+}/Ca^{2+}$ Exchanger Modulates $Ca^{2+}$-Dependent Exocytotic Release of Glutamate from Rat Cortical Astrocytes. DOI: 10.1042/AN20110059

23. C Agulhon et al., (2008): What Is the Role of Astrocyte Calcium in Neurophysiology? DOI: 10.1016/j.neuron.2008.09.004.
24. Codazzi et al., (2001): Control of astrocyte $Ca^{2+}$ oscillations and waves by oscillating translocation and activation of protein kinase C. DOI: 10.1016/S0960-9822(01)00326-8
25. Parri and Crunelli (2003): The role of Ca2+ in the generation of spontaneous astrocytic Ca2+ oscillations. DOI: 10.1016/s0306-4522(03)00379-8
26. JJ Omoto (2016): Origins of glial cell populations in the insect nervous system. DOI: 10.1016/j.cois.2016.09.003